Article

Programmable Modulation of Copper Naonoclusters Electrochemiluminescence via DNA Nanocranes for Ultrasensitive Detection of microRNA

Ying Zhou, Haijun Wang, Han Zhang, Ya-Qin Chai, and Ruo Yuan

Anal. Chem., **Just Accepted Manuscript** • DOI: 10.1021/acs.analchem.7b05402 • Publication Date (Web): 05 Feb 2018

Programmable Modulation of Copper Naonoclusters Electrochemiluminescence *via* DNA Nanocranes for Ultrasensitive Detection of microRNA

Ying Zhou, Haijun Wang, Han Zhang, Yaqin Chai*, Ruo Yuan*

Key Laboratory of Luminescent and Real-Time Analytical Chemistry (Southwest University), Ministry of Education, College of Chemistry and Chemical Engineering, Southwest University, Chongqing 400715, PR China

*Corresponding authors at: Tel.: +86 23 68252277, fax: +86 23 68253172.
E-mail addresses: yqchai@swu.edu.cn (Y. Q. Chai), yuanruo@swu.edu.cn (R. Yuan).

ABSTRACT

The DNA nanocrane with functionalized manipulator and fixed-size base offered a programmable approach to modulate the luminous efficiency of copper naonoclusters (Cu NCs) for achieving remarkable electrochemiluminescence (ECL) enhancement, further the Cu NCs as signal label was constructed in biosensor for ultrasensitive detection of microRNA-155. Herein, the DNA nanocrane was first constructed by combining of binding-induced DNA assembly as manipulator and tetrahedral DNA nanostructure (TDN) as base, which harnessed a small quantity of specific target (miRNA-155) binding to trigger assembly of separate DNA components for producing numerous AT-rich double-stranded DNA (dsDNA) on the vertex of TDN. Upon the incubation of Cu^{2+} on the AT-rich dsDNA, each DNA-stabilized Cu NCs probe could be in situ electrochemically generated on an individual TDN owing to the A-Cu^{2+}-T bond. Thus, the generation of Cu NCs was highly regulated with AT-rich dsDNA as the template, and its lateral distance was tuned by the TDN size, which were two key factors to influence the luminous efficiency of Cu NCs. By coordinate modulation, the detection limit of the ultrasensitive biosensor for miRNA-155 down to 36 aM and the programmable modulation strategy paved the way for comprehensive applications of DNA nanomachines and metal nanoclusters in biosensing and clinical diagnosis.

KEYWORDS: electrochemiluminescence; DNA nanocranes; Cu nanoclusters; miRNA detection;

INTRODUCTION:

With the size approaching the electron Fermi wavelength, the spatial confinement of free electrons in metal nanoclusters (NCs) generates discrete and size-tunable electronic transitions, leading to unique optical properties including fluorescence [1-3]

and electrochemiluminescence (ECL) [4-6]. During the past decade, the researchers have enabled facile synthesis of metal NCs in various biocompatible scaffolds, establishing them as a new class of ultrasmall, biocompatible luminophor for applications as biological labels or optoelectronic emitters [7-10]. Ying and coworkers has reported BSA as large and complicated proteins possess abundant binding sites to bind novel metal ions, thus offering better scaffolds for template-driven formation of small metal NCs [11]. Although metal NCs in protein template have obtained significant ECL signals due to abundant immobilization of signal labels, the ECL efficiency of these metal NCs was still restricted, because the tight molecular arrangement of metal NCs would increase inner filter effect and impede the electrochemical activation of the internal ECL emitters [12-14]. More recently, Ouyang et al developed the sequence-dependent synthesis of Cu NCs *via* the stable A-Cu^{2+}-T bond, in which the longitudinal distribution of Cu NCs could be controlled onto DNA templates [15], but the modulation of their lateral distance has not been realized. Owing to the highly specific Watson-Crick base pairing, DNA molecules can be self-assembled into various DNA nanomachines with high predictability and precision [16-18]. Here, the well-defined DNA nanocrane was designed for the oriented immobilization of Cu NCs to programmably tune the sequence-dependent formation and lateral distance for studying their ECL efficiency.

MiRNAs are a class of short noncoding RNAs (18 to 25 nucleotides), acting as sequence-specific post-transcriptional regulators, which play critical roles in human cellular network. [19-21] Recently, many researches have focused on the convergent and cooperative miRNA network that drives angiogenesis and tumor metastasis. Developing a highly sensitive method for miRNA detection is of great clinical significance. [22, 23] Herein, an ultrasensitive biosensor was constructed for miRNA-155

detection based on DNA nanocranes engineered amplification platform, which was construct by the combination of tetrahedral DNA nanostructure (TDN) as base and binding-induced DNA assembly as manipulator. As shown in Scheme 1, when the inactive DNAzyme motor (DNA_1) interacted with the target molecule, the target miRNA-155 could hybridize with the locking strand (DNA_2) through a strand displacement reaction, forming DNA_1-DNA_3 duplex structure. Subsequently, the Mn^{2+} DNAzyme-assisted target recycling was triggered to drive DNA walker and cleave DNA_3 to reuse the target and release product DNA (Apt_1). By design, the Apt_1 was composed of a short sequence **P*** (8AT), tandem periodic AT sequence and ATP recognition sequence. ATP aptamer 2 (Apt_2) containing ATP recognition sequence was anchored on the vertex of TDN_2 modified sensing surface. Thus, the binding of ATP with Apt_1 and Apt_2 brought the **P*** sequence of Apt_1 into close proximity with the **P** sequence of TDN_1 for forming the **P:P*** hybrid. With the aid of phi29 and deoxynucleotides (dNTPs), the **P:P*** hybrid triggered the DNA polymerization by Apt_1 as the circular template, producing AT-rich double-stranded DNA (dsDNA). When dsDNA polymerization of Apt_1 completed, Apt_2 and ATP were detached from Apt_1 and drove to move autonomously along the sensing surface until all dsDNAs were produced. Furthermore, the AT-rich dsDNAs could be acted as ligands to in situ electrochemically generate Cu NCs on the vertex of TDN_1, when the dsDNA was incubated with $CuSO_4$ solution to form the stable A-Cu^{2+}-T bond. Therefore, the particle size and lateral spacing of Cu NCs were respectively tuned by the distribution of AT sequence and the fixed size of TDN, which profoundly promoted ECL emission of Cu NCs due to the more loading capacity and less collision loss. As a result, the biosensors based DNA nanocranes exhibited a wide linear range from 100 aM to 100 pM with a low detection limit of 36 aM for miRNA-155. The success in the

establishment of the DNA nanocranes revealed a new avenue for the development of ultrasensitive biosensors by incorporating multiple leading edged techniques.

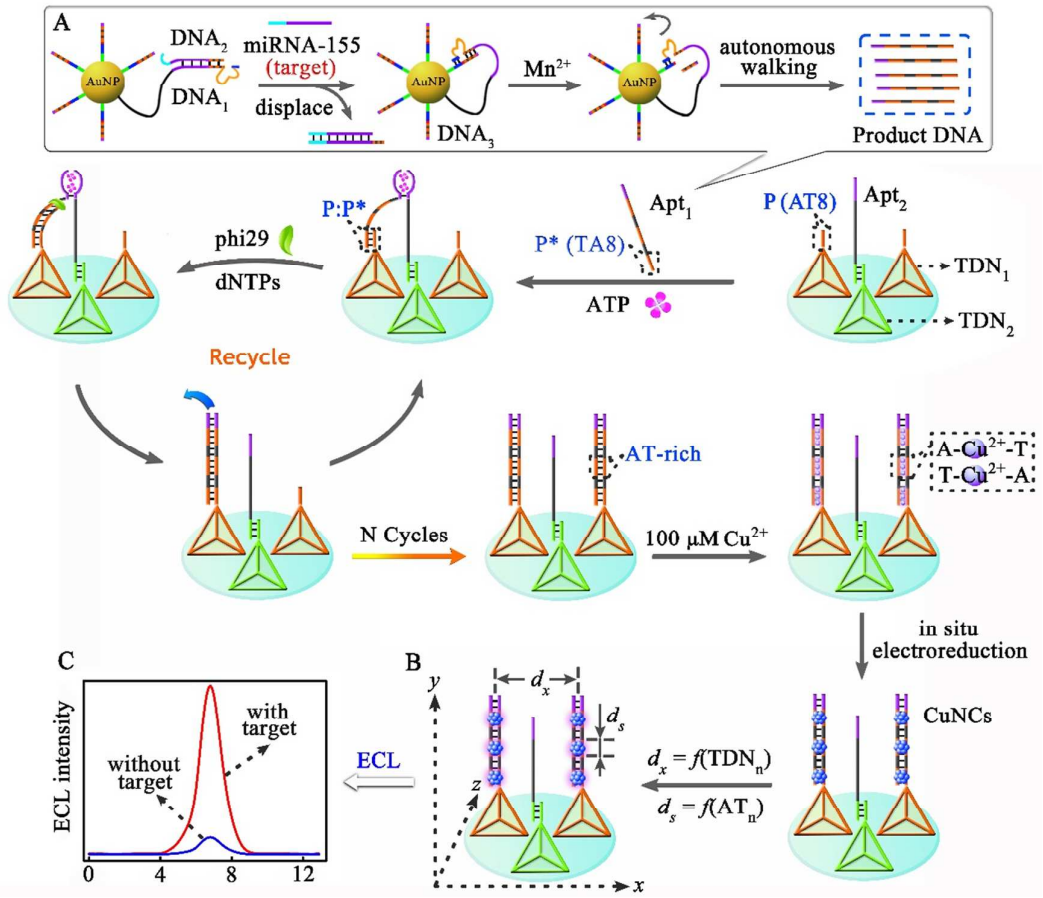

Scheme 1. Schematic illustration of the nanocranes based-biosensor: (A) The target-nucleotide transduction-amplification strategy; (B) Programmable modulation of the ECL efficiency of Cu NCs; (C) Signal comparison of miRNA-155 detection. (d_x = the lateral spacing of Cu NCs, d_s = the particle size of Cu NCs).

EXPERIMENTAL SECTION

Assembling of TDN scaffolds. In this work, tetrahedral DNA nanostructure (TDN) were formed by one-pot incubation technique with a simple annealing process [24, 25]. At the beginning, equimolar amounts of the four constituent oligonucleotides (A, B, C and D ssDNA, the sequences in the supporting information) were combined in TM buffer (10 mM Tris-HCl, 35 mM $MgCl_2$, pH 8.0). The hybridization mixture was heated at 95 ºC for 5 min and then cooled to room temperature over 24 h. High

temperature could effectively make DNA chain denatured to an open end and improve the hybridization of DNA to expectant structures in the process of temperature reduction. Once assembled, the TDN contained specific branched DNA at one edge and three COOH groups at other three vertices. Finally, the obtained TDN were purified by ultra-filtration (30 K molecular weight cutoff) to remove the non-conjugated oligonucleotides.

Signal Transduction and Amplification for miRNA-155 Detection. The Mn^{2+}-DNAzyme assisted target recycling strategy [26] was constructed by functionalizing AuNP with pre-locked DNAzyme (DNA_1-DNA_2) and DNA_3 *via* Au-S bond. Specifically, DNA_1 and DNA_2 at a molar ratio of 1:3 were mixed in PBS buffer (pH 7.4) to ensure the preparation of locked DNAzyme strand. Specifically, 16-nm AuNPs, locked DNAzyme strand (DNA_1-DNA_2) and DNA_3 were mixed at a molar ratio of 1: 50: 1000, and incubated at room temperature overnight. Subsequently, the functionalized AuNPs could be collected by centrifugation by using Tris-HCl (10 mM, pH 7.4) containing 0.05% Tween 20. Then 95 μL of above solution was incubated with different concentrations target (miRNA-155) at room temperature for 30 min, Mn^{2+} (5 μL, 10 mM) was added to initiate the operation of DNA_1 (DNA walker) and cleave DNA_3 for 60 min. Finally, the mixture solution was separated by centrifugation to obtain product DNA (Apt_1) with different concentrations for further immobilization on the modified electrode surface.

Fabrication of Biosensor. Before modification, the GCE (Φ = 4 mm) was continuously polished with 0.3 and 0.05 mm alumina slurry and then cleared thoroughly with deionized water in the ultrasonic apparatus. At first, 5 μL of amino-modified Fe_3O_4@CeO_2 solution was directly immobilized onto the clear electrode surface. After drying, 4 μL of 2 μM carboxyl-modified TDN_1 and 1 μL of 2

μM carboxyl-modified TDN_2 were respectively incubated on the electrode *via* amidation reaction for 6 h at 4 ºC. Following that, 1 μL Apt_2 (5 μM) was dripped onto the GCE for 12 h at room temperature to form Apt_2-TDN_2 on the above prepared electrode. After blocking, 5 μL Apt_1 from miRNA-155 transduction, 2 μL ATP (10 μM) and 3 μL phi29 buffer (33 mM Tris-acetate, 10 mM Mg-acetate, 66 mM K-acetate, 1 mM DTT, pH 7.5) containing phi 29 (100 U/mL) and dNTPs (200 μM) were dropped onto the modified electrode and incubated for 3 h at room temperature.

ECL Measurement Procedure. Subsequently, the modified biosensors were incubated with 10 μL of 100 μM $CuSO_4$ solution for 60 min when AT-rich dsDNAs were generated. After rinsing with deionized water to remove the unbound copper ions, the potential from 0 to −2 V with a scan rate of 300 mV/s was applied to the biosensor for in situ electrochemical reduction of Cu NCs. As a result, the proposed biosensors were measured in 0.1 M PBS (pH 7.4) containing 5 mM $K_2S_2O_8$. The construction of the proposed biosensor, the AT-rich dsDNA polymerization and programmable modulation of the ECL efficiency of Cu NCs were detailedly presented in Scheme 1. The electrochemical performance of the biosensor was investigated by cyclic voltammetry (CV) measurements, and shown in the supporting information.

RESULTS AND DISCUSSION

Characterization of in Situ Electrochemical Generation of Cu NCs. HRTEM was carried out to investigate the morphology of the in situ generated Cu NCs on dsDNA (Figure 1A). It could be seen that Cu NCs were mainly distributed in the range 1.0-2.5 nm with an average diameter of 1.5 nm. Subsequently, we explored photophysical characterizations of DNA-stabilized Cu NCs. The biosensor was measured in 0.1 M PBS (pH 7.4) containing 5 mM $S_2O_8^{2-}$ by scanning the potential from 0 to −2.0 V, three distinct reduction peaks could be clearly observed from the

CV curve of Figure 1B. The first two peaks at around −0.59 V and −0.96 V respectively reflected the electrochemical generation of Cu NCs and the reduction reaction of $S_2O_8^{2-}$. And the last peak at −1.39 V corresponded to the reduction reaction of Cu NCs [27]. Figure 1C displayed the UV-vis absorption spectra of the AT-rich dsDNA (curve a) and the dsDNA-stabilized Cu NCs (curve b). As shown in curve a, a distinct absorption peak was observed at 285 nm, which was the specific absorption peak of DNA [28, 29]. After the in situ generation of Cu NCs, the specific absorption peak became broader and had a slightly blue-shift of 17 nm comparing with that of dsDNA (curve b), attributing to quantum size effect of Cu NCs [30]. The luminescence of the Cu NCs was profiled with the photoluminescence (PL) spectra and the ECL spectra. Figure 1D depicted the PL emission peak of the Cu NCs at 390 nm (curve a). Meanwhile, the ECL spectra was located around 424 nm (curve b), which significantly differed from the emission peak of a typical $S_2O_8^{2-}/O_2$ ECL system (around 575 nm, from Figure S1). The result manifested that the ECL signal came from the emission of Cu NCs rather than the $S_2O_8^{2-}/O_2$ ECL system. The slight red shift from the PL spectrum to ECL spectrum was attributed to the self-absorption of Cu NCs and instrument effects [31, 32].

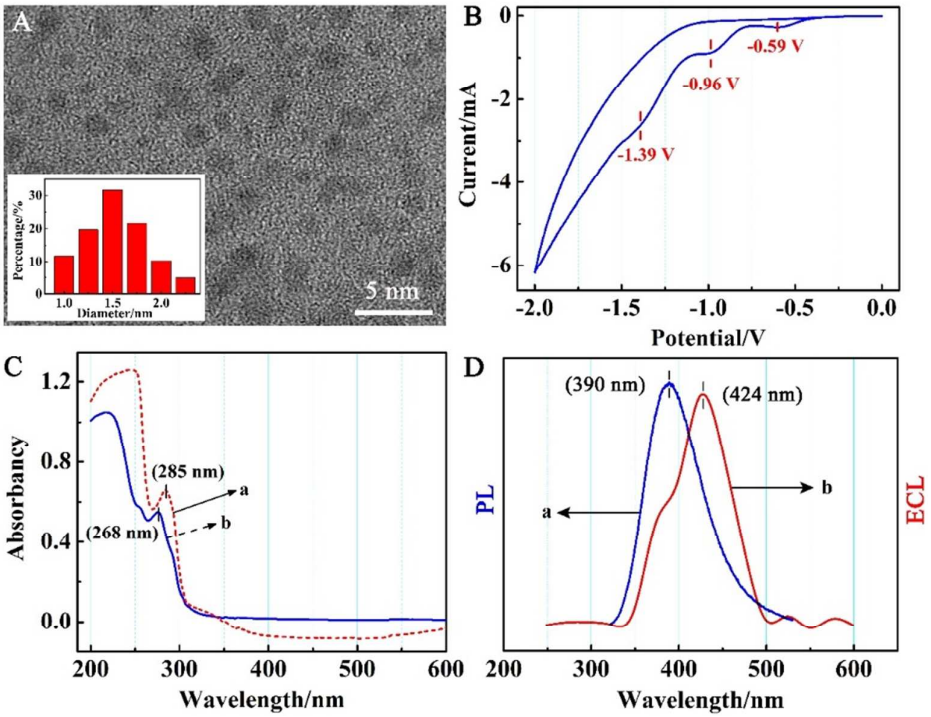

Figure 1. (A) HRTEM images of the Cu NCs in situ generated on AT-rich dsDNA. (B) Typical CV curve of the in situ Cu NCs generation. (C) UV-vis absorption profiles of the AT-rich dsDNA ligands (curve a) and DNA-stabilized Cu NCs (curve b). (D) PL emission spectrum (curve a) and normalized ECL spectra of Cu NCs (curve b). The ECL signal was measured in 0.1 M PBS (pH 7.4) containing 5 mM $S_2O_8^{2-}$.

Mechanism of the DNA Nanocrane Operation. We designed that the DNA nanocrane was consist of binding-induced DNA assembly as manipulator and TDN as base. First, ATP binding triggered the **P*** sequence of Apt_1 into close proximity with the **P** sequence of TDN_1 for forming the **P:P*** hybrid. As displayed in Figure 2A, the **P:P*** hybrid as the recognition site triggered the DNA polymerization with the help of phi29 and dNTPs, which could extend the complementary pair from the 3'-terminus of the **P** sequence in the 3'-to-5' direction. Thus the new complementary strand (the red sequence) hybridized with Apt_1 (the purple sequence) to form dsDNA and simultaneously displaced Apt_2 (the blue sequence) and ATP. The liberated ATP again associated with another Apt_1 and Apt_2 until all AT-rich dsDNAs were generated and the nanocrane stopped.

Upon the incubation of Cu^{2+} on the generated dsDNA, the Cu NCs could be in situ electrochemical reduced on the dsDNA templates, the biosensor exhibited increasing ECL intensity. Therefore, we could be able to monitor the nanocrane operation by detecting the ECL of the Cu NCs (Figure 2B). The same batch of biosensors were incubated with Apt_1 from 100 fM miRNA-155 transduction, and then measured once every 25 min to record corresponding ECL intensity. The progress curve revealed that the nanocrane operated in three phases to test the feasibility of the nanocrane. Once activated, the biosensor exhibited ECL at an initial linear rate for about 2 h (phase 1). The enzymatic polymerization of dsDNA followed steady-state kinetics. After a large fraction of dsDNA polymerization completed, fewer TDN_1 with **P** were available for hybridization to **P*** and the nanocrane operation became slower (phase 2). Finally, when no spare **P** on TDN_1 is accessible by **P*** of the Apt_1, the operation of nanocrane completed and the ECL intensity reached to a plateau after 2.75 h (phase 3). Therefore, 3 h was chosen for the polymerization time in this study.

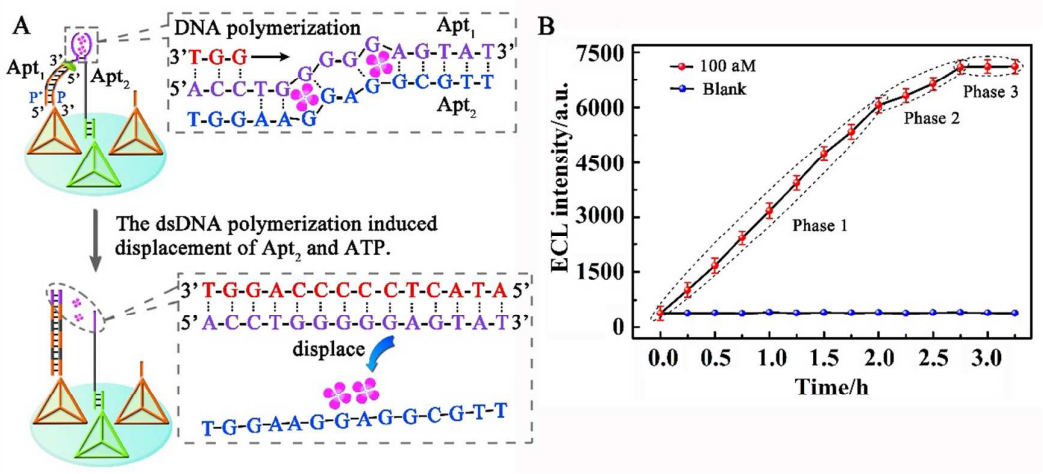

Figure 2. (A) The dsDNA polymerization induced separation of Apt_2 and ATP. (B) Typical progress curve indicated three phases of the nanocrane operation.

ECL Performance of TNDs Modified Sensing Strategies. After understanding the DNA nanocrane operation process, the generation of Cu NCs was regulated by

altering the distribution of AT sequence in the dsDNA templates to obtain efficient ECL emission. First, the Apt_1 (from miRNA-155 transduction) was designed to contain 55 nucleotides so that it could provide sufficient spatial distance for constructing the high efficient nanocrane. Subsequently, the sizes of Cu nanoparticles (NPs) were tuned by same total full-length templates but different AT sequence distributions based on the A-Cu^{2+}-T bond. The characterization and ECL property of Cu NPs were researched *via* ECL and HR-TEM. As shown in the Figure 3A, the highest ECL peak intensity was achieved from the AT8-dsDNA-stabilized Cu NCs (*a*). Figure S3B showed that the Cu NPs with the non-consistent size were synthesized in the template of AT4-dsDNA (*b*), while Figure S3C displayed that the Cu NPs tended to reunite in the template of AT16-dsDNA (*c*). This implies that control of the particle size is a powerful strategy to modulate ECL properties of NCs.

Furthermore, TDN-12, TDN-18, TDN-24, and TDN-30 were employed for regulating the lateral distance between probes (dsDNA stabilized Cu NCs) to decrease the inner filter effect and minimize inactive emitters, in which each edge of the TDN contained 12, 18, 24 or 30 base pairs, respectively. Because each base pair was separated by 0.34 nm in a double helix, the lateral distances between probes were approximately calculated to be 4.08, 6.12, 8.16, and 10.2 nm. Native polyacrylaimide gel electrophoresis (PAGE) analysis showed that the TDN could be self-assembled with relative high yields (Figure S4). The same batch of biosensors were modified on four types of TDNs, and then a segment of the DNA probe was carried at one vertex of each TDN (Figure 3B). Simultaneously, the DNA probes were directly immobilized on sensing interface to act as the control group (Blank). After incubating with Cu^{2+}, five kinds of biosensors were measured once every five minutes to record corresponding ECL intensity. As shown in the inset II of Figure 3, the ECL signals

increased with the increasing incubation time from 0 min to 70 min, and then reached to a plateau after 60 min, suggesting that 60 min was enough for Cu NCs generation. The Cu NCs based TDN-24 had a more significant rise and processed always a higher ECL intensities comparing with other Cu NCs. More significantly, The Cu NCs based TDN-24 also had high efficiency of ECL (Φ_{ECL}, the inset I of Figure 3), in which Φ_{ECL} was defined as the number of photons per electron transferred (the detailed calculation procedure shown in the supporting information). When the lateral distance of ECL probes at about 8 nm (the edge length of two TDNs-24), the Cu NCs has excellent ECL performance, due to less inner filter effect and more electrochemical activation. According to experimental results, the use of DNA nanocrane not only improved the probe spacing to form more Cu NCs, but significantly reduced the collision annihilation of excited state species Cu NCs*, which remarkably improved the ECL efficiency of Cu NCs. (All DNA sequences shown in the supporting information)

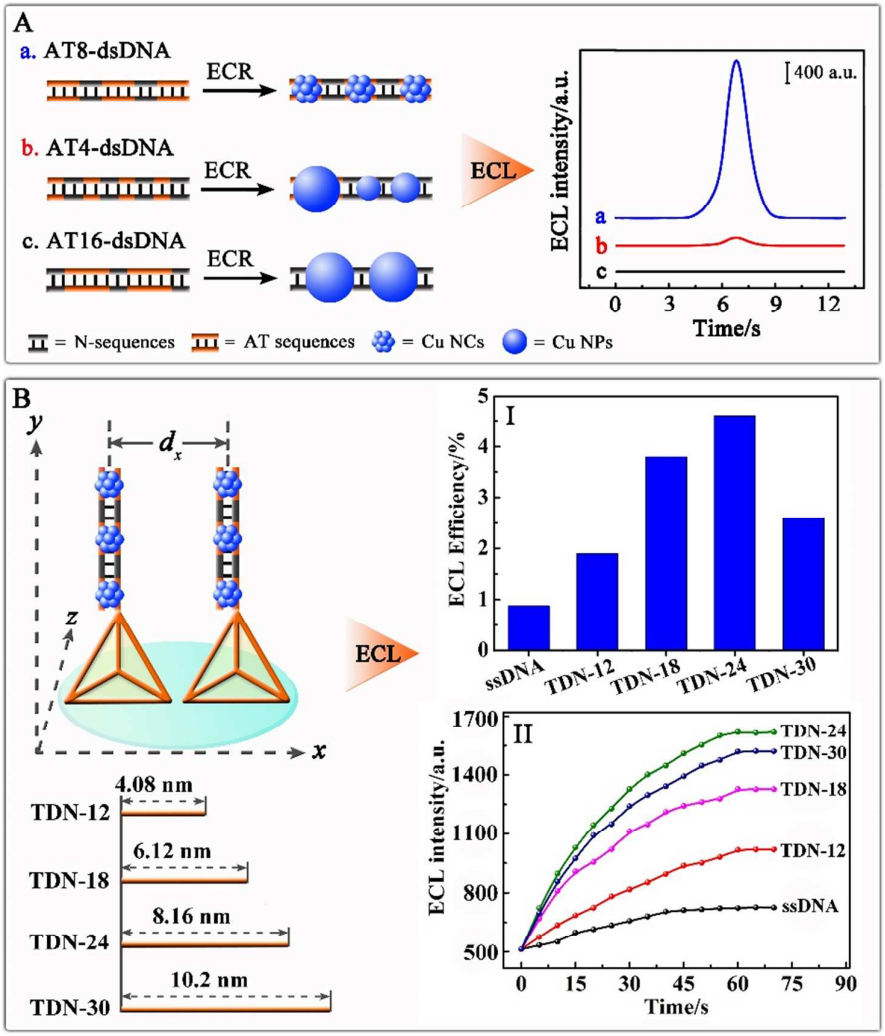

Figure 3. The schematic diagrams showed programmable modulation of Cu NCs. (A) The particle sizes of Cu NCs were regulated through the different distribution of AT sequence in dsDNA templates (electrochemical reduction: ECR); (B) The lateral distances between probes were tuned by differently sized TDNs, and four types of TDNs with different sizes were designed; (I) The ECL efficiency and (II) the ECL intensity of the biosensors with the differently sized TDNs or dsDNA (blank) were investigated.

Analytical Performance. Under the optimal reaction conditions, the proposed biosensors were successively detected in 0.1 M PBS (pH 7.4) containing 5 mM $S_2O_8^{2-}$ by scanning the potential from 0 to −2.0 V at a scanning rate of 300 mV/s. As exhibited in Figure 4A, the ECL intensity of Cu NCs increased with increasing concentration of miRNA-155 from100 aM to 100 pM (curves a~g) and presented an excellent linear relationship with the logarithm of concentration. The regression

equation was I = 2292.4 lg$c$ + 10605, where I was the obtained ECL intensity and c was the miRNA-155 concentration. Moreover, the limit of detection was calculated to be 36 aM according to the equation of LOD=3S_b/m (S_b is the standard deviation of the blank intensity and m is the slope of the calibration). The comparison for existing miRNA detection bioanalysis indicated the prepared biosensor exhibited better sensitivity (Table S1). It could be attributed that the programmable modulation profoundly promoted ECL emission of Cu NCs due to the more loading capacity and less collision loss.

The selectivity of the ECL biosensor for miRNA-155 was demonstrated by opposing other interferences of miRNA-21, miRNA-141, miRNA-199a. From the results in Figure 4C, it could be seen that the ECL intensities of miRNA-21 (10 pM), miRNA-141 (10 pM), miRNA-199a (10 pM) significantly decreased comparing with that of the interference experiment at the presence of miRNA-155 (100 fM). Meanwhile, there were no obvious changes between the ECL responses obtained in the mixture solution (100 fM miRNA-155 containing 10 pM miRNA-21, 10 pM miRNA-141, and 10 pM miRNA-199a) and that obtained in pure miRNA-155 (100 fM). Subsequently, the stability as one of important factors was investigated by employing the biosensor for consecutive cyclic scans, which was evaluated for the proposed biosensor incubated with various concentration of miRNA-155 (Figure 4D). It could be found that relative stable curves could be obtained for the proposed biosensor on every concentration of miRNA-155, indicating the excellent stability of the biosensor. Meanwhile, the assay approach showed potential applications in clinical diagnostics, and the clinical serum samples analysis was depicted in Table S2.

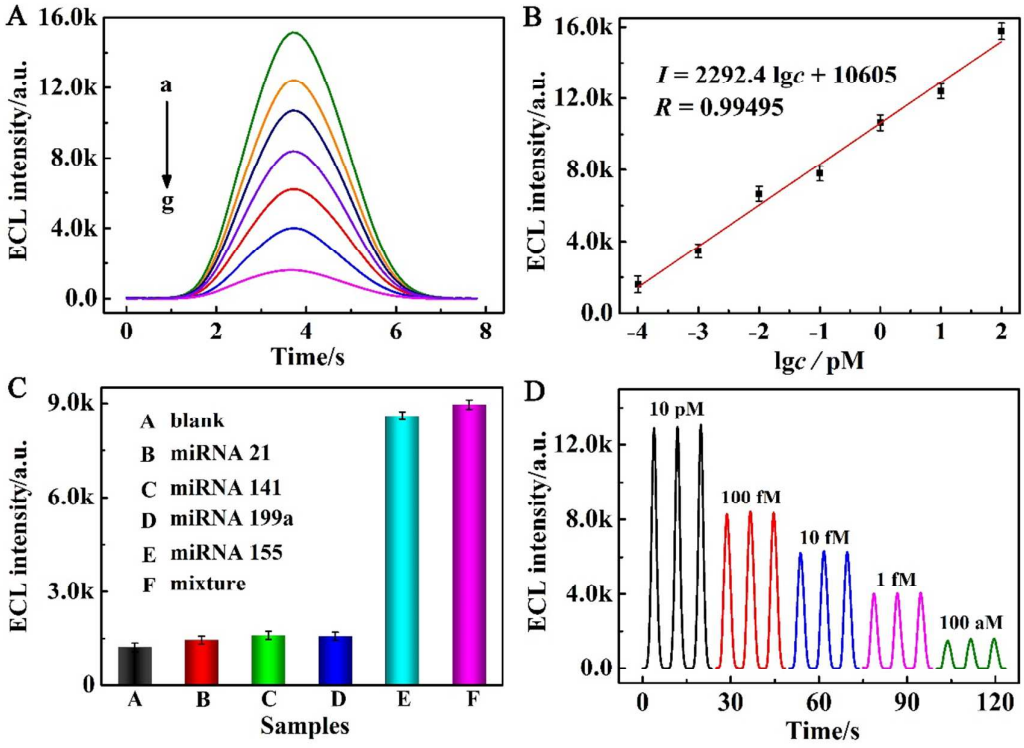

Figure 4. (A) ECL profiles of the biosensor incubating miRNA-155 with different concentrations: 100 aM, 1 fM, 10 fM, 100 fM, 1 pM, 10 pM, and 100 pM. (B) Calibration plots of the proposed biosensor. (C) Selectivity of the biosensor detection of miRNA-155 (100 fM) against the interference miRNA: miRNA-21, miRNA-141, and miRNA-199a. (D) The ECL stability of the proposed biosensor to various concentrations of miRNA-155.

CONCLUSION

In summary, the present work first constructed novel DNA nanocranes based on binding-induced DNA assembly as manipulator and TDN as base and its application of the Cu NCs-based sensing platform for the ultrasensitive detection of miRNA-155. This study had brought forth the following three novel ideas. First, the binding-induced DNA assembly finely manipulated the generation of AT-rich dsDNA. Based on the stable A-Cu^{2+}-T, the DNA nanocranes realized a small quantity of miRNA-155 triggered the generation of a large amount of Cu NCs. Second, TDN could not only improve the probe spacing to generate more Cu NCs, but also lessen collision annihilation of excited state species Cu NCs* for retaining remarkable ECL

emitting, which significantly promoted the sensitivity of the biosensor. Third, the reasonable-designed biosensor simultaneously realized activity modulation of ECL probes (the DNA-stabilized Cu NCs) and target recycling amplification, achieving ultrasensitive analysis of miRNA-155 with the detection limit of 36 aM. With the ingenious combination of DNA nanocranes, the proposed biosensor exhibited excellent selectivity, accuracy and stability and provided a dynamic sensing platform for various target analysis in diverse applications, such as early disease diagnose and environmental analysis.

ASSOCIATED CONTENT

Experimental details for chemicals and apparatus, DNA sequences employed in the proposed biosensor, preparation of amino-modified Fe_3O_4@CeO_2, optical spectrum sharacterization of $S_2O_8^{2-}/O_2$ ECL system, experimental condition optimization, characterization of the ECL biosensor, ECL efficiency of the Cu NCs, the HR-TEM image of dsDNA-CuNPs, native PAGE characterization of TDN nanostructure, limit of detection calculation, comparison of this work with the previous research, and application of the biosensor are provided as Supporting Information. This material is available free of charge via the Internet at http://pubs.acs.org.

AUTHOR INFORMATION

* Corresponding authors

Tel.: +86 23 68252277, fax: +86 23 68253172.

E-mail addresses: yqchai@swu.edu.cn (Y. Q. Chai), yuanruo@swu.edu.cn (R. Yuan).

Notes

The authors declare no competing financial interest.

ACKNOWLEDGMENT

This work was financially supported by the National Natural Science Foundation (NNSF) of China (Grants 21675130, 21575116 and 51473136), the Fundamental Research Funds for the Central Universities (Grant XDJK2017A001), and Chongqing Postdoctoral Science Foundation (Xm2017016).

REFERENCES

(1) Nonappa; Lahtinen, T.; Haataja, J. S.; Tero, T.; Häkkinen, H.; Ikkala, O. *Angew. Chem. Int. Ed.* **2016**, 55, 16035-16038.

(2) Copp, S. M.; Bogdanov, P.; Debord, M.; Singh, A.; Gwinn, E. *Adv. Mater.* **2014**, 26, 5839-5845.

(3) Cao, S.; Ding, S.; Liu, Y.; Zhu, A.; Shi, G. *Anal. Chem.* **2017**, 89, 7886-7892.

(4) Swanick, K. N.; Hesari, M.; Workentin, M. S.; Ding, Z. *J. Am. Chem. Soc.* **2012**, 134, 15205-15208.

(5) Hesari, M.; Workentin, M. S.; Ding, Z. *Chem. Sci.* **2014**, 5, 3814-3822.

(6) Zhang, L.; Wang, E. *Nano Today,* **2014**, 9, 132-157.

(7) Chen, T.; Hu, Y.; Cen, Y.; Chu, X.; Lu, Y. *J. Am. Chem. Soc.,* **2013**, 135, 11595-11602.

(8) Shang, L.; Dong, S.; Nienhaus, G. U. *Nano Today,* **2011**, 6, 401-418.

(9) Tanaka, S. I.; Miyazaki, J.; Tiwari, D. K. *Angew. Chem. Int. Ed.,* **2011**, 50, 431-435.

(10) Hesari, M.; Workentin, M. S.; Ding, Z. *ACS Nano* **2014**, 8, 8543-8553.

(11) Xie, J.; Zheng, Y.; Ying, J. Y. *J. Am. Chem. Soc.* **2009**, 131, 888-889.

(12) Tian, R.; Zhang, S.; Li, M.; Zhou, Y.; Lu, B.; Yan, D.; Wei, M.; Evans, D. G.; Duan, X. *Adv. Funct. Mater.* **2015**, 25, 5006-5015.

(13) Zhou, Y.; Wang, H. J.; Zhuo, Y.; Chai, Y. Q.; Yuan, R. *Anal. Chem.* **2017**, 89, 3732-3738.

(14) Shang, L.; Brandholt, S.; Stockmar, F.; Trouillet, V.; Bruns, M.; Nienhaus, G. U. *Small* **2012**, 8, 661-665.

(15) Song, Q.; Shi, Y.; He, D.; Xu, S.; Ouyang, J. *Chem. Eur. J.* **2015**, 21, 2417-2422.

(16) Modi, S.; Nizak, C.; Surana, S.; Halder, S.; Krishnan, Y. *Nature Nanotech.,* **2013**, 8, 459-467.

(17) Liu, H.; Shen, F.; Haruehanroengra, P. *Angew. Chem. Int. Ed.* **2017**, 56, 9430-9434.

(18) Xie, N.; Huang, J.; Yang, X.; He, X.; Liu, J.; Huang, J.; Fang, H.; Wang, K. *Anal. Chem.* **2017**, 89, 12115-12122.

(19) Fabian, M. R.; Sonenberg, N.; Filipowicz, W. *Ann. Rev. Biochem.* **2010**, 79, 351-379.

(20) Aguda, B. D.; Kim, Y.; Piper-Hunter, M. G.; Friedman, A.; Marsh, C. B. *Proc. Natl. Acad. Sci. U. S. A.* **2008**, 105, 19678-19683.

(21) Zhang, Y. C.; Yu, Y.; Wang, C. Y.; Li, Z. Y.; Liu, Q.; Xu, J.; Liao, J. Y.; Wang, X. J.; Qu, L. H.; Chen, F.; Xin, P. Y.; Yan, C. Y.; Chu, J. F.; Li, H. Q.; Chen, Y. Q. *Nat. Biotechnol.* **2013**, 31, 848-852.

(22) Gai, P.; Gu, C.; Li, H.; Sun, X.; Li, F. *Anal. Chem.* **2017**, 89, 12293-12298.

(23) Persson, H.; Sokilde, R.; Hakkinen, J.; Pirona, A. C.; Vallon-Christersson, J.; Kvist, A.; Mertens, F.; Borg, A.; Mitelman, F.; Hoglund, M.; Rovira, C. *Nat. Commun.* **2017**, 8, 788.

(24) Lu, N.; Pei, H.; Ge, Z.; Simmons, C. R.; Yan, H.; Fan, C. H. *J. Am. Chem. Soc.,* **2012**, 134, 13148-13151.

(25) Shao, X.; Lin, S.; Peng, Q.; Shi, S.; Wei, X.; Zhang, T.; Lin, Y. *Small* **2017**, 13, 1602770.

(26) Peng, H.; Li, X.-F.; Zhang, H.; Le, X. C. *Nat. Commun.* **2017**, 8,14378.

(27) Härtinger, S.; Rosenmund, J.; Savinova, E.; Wasle, S.; Doblhofer, K. *J. Phys. Chem. B* **1997**, 101, 2411-2414.

(28) O'Neill, P. R.; Gwinn, E. G.; Fygenson, D. K. *J. Phys. Chem. C* **2011**, 115, 24061-24066.

(29) Niehaus, M.; Schnapp, A.; Koch, A.; Soltwisch, J.; Dreisewerd, K. *Anal. Chem.* **2017**, 89, 7734-7741.

(30) Zhou, Z. X.; Du, Y.; Dong, S. J. *Anal. Chem.* **2011**, 83, 5122-5127.

(31) Linic, S.; Christopher, P.; Ingram, D. B. *Nature Mater.* **2011**, 10, 911-921.

(32) Rashidnadimi, S.; Hung, T. H.; Wong, K. T.; Bard, A. J. *J. Am. Chem. Soc.* **2008**, 130, 634-639.

For TOC only

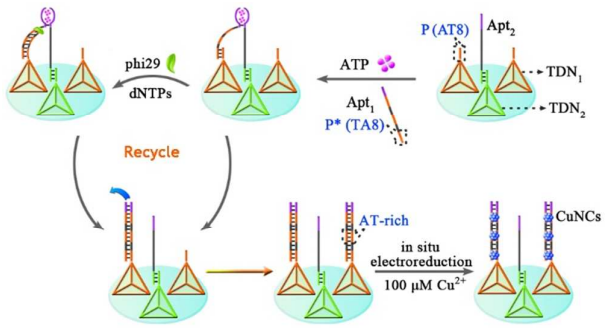
phi29
dNTPs
ATP
P (AT8)
Apt2
TDN1
TDN2
Apt1
P* (TA8)
Recycle
AT-rich
in situ
electroreduction
100 μM Cu2+
CuNCs